Applied Surface Science 265 (2013) 379–384

Contents lists available at SciVerse ScienceDirect

Applied Surface Science

journal homepage: www.elsevier.com/locate/apsusc

Co_3O_4/ZnO nanocomposites for gas-sensing applications

Yuanjun Liu[a], Guoxing Zhu[b], Junzhi Chen[a], Huan Xu[b], Xiaoping Shen[b], Aihua Yuan[a,*]

[a] School of Biology and Chemical Engineering, Jiangsu University of Science and Technology, Zhenjiang 212003, China
[b] School of Chemistry and Chemical Engineering, Jiangsu University, Zhenjiang, 212013, China

ARTICLE INFO

Article history:
Received 3 June 2012
Received in revised form 1 November 2012
Accepted 5 November 2012
Available online 10 November 2012

Keywords:
ZnO
Co_3O_4
p–n junction
Gas sensor
Nanocomposites

ABSTRACT

Co_3O_4/ZnO nanocomposites were prepared by an easy wet-chemistry route without any organic additive or surfactant used. The nanocomposites were systematically characterized by X-ray powder diffraction, scanning electron microscopy, (high-resolution) transmission electron microscopy, selected area electron diffraction, and energy-dispersive X-ray spectroscopy. The results show that ZnO is loaded on the surface of Co_3O_4 nanoparticles with a compact and clean hetero-interface. The obtained nanocomposites were tested for gas-sensing applications with ethanol and formaldehyde as model gases. It was revealed that the nanocomposites exhibit enhanced gas-sensing performance such as high stability and high sensing response. The sensing responses to 100 ppm ethanol or formaldehyde (46 to ethanol and 20 to formaldehyde) are much higher than those of pristine Co_3O_4 nanoparticles (6.2 to ethanol and 4.4 to formaldehyde), commercial Co_3O_4 powder (1.6 to ethanol and 1.5 to formaldehyde), and pure ZnO sample (7.5 to ethanol and 4.1 to formaldehyde). These results suggest that the integration of Co_3O_4 with ZnO is a promising route to the development of effective sensing materials. The excellent gas-sensing properties and the easily up-scalable preparation route make the prepared nanocomposites be promising for real applications.

1. Introduction

Metal oxide nanostructures as sensing materials have been widely investigated because of their promising applications in detecting various gaseous and volatile chemicals, such as hydrazine, methanol, chloroform, dichloromethane, acetone, ethanol, etc. [1–3]. The gas sensing behavior of metal oxide is usually measured based on the resistance change caused by tested gases. p-Type metal oxide semiconductors often have lower sensing responses than n-type metal oxide semiconductors [1,2]. However, in some special cases of electrical circuits, a sensor based on a p-type metal oxide semiconductor is required.

To improve the sensing response, one route involves the shape and size control of sensing materials [1,2,4–6]. The shape and size of sensing materials considerably influence their sensing performance by the variation of the surface lattice plane caused by different particle shapes, and/or by changing the surface area caused by different particle sizes. To date, much effort has been devoted to the investigation of the morphology- and/or size-dependent sensing properties. Another method to improve sensing response is the introduction of second species to form composites. Noble metal nanoparticles such as Pt, Pd, Au, and Ag are often chosen and loaded on the surface of metal oxides [7–10]. These nanoparticles act as adsorption sites for analytes or as surface catalyst for sensing. However, noble metals are expensive, and thus it is desirable to develop economical second materials for improving the sensing performances. It is well known that the combination of a *p*-type semiconductor (such as Co_3O_4) with an *n*-type semiconducting oxide can form a p–n junction. The p–n junction has recently garnered increasing attention because of its superior performances in photocatalytic and optoelectronic applications, and the superior performance of the p–n junction is attributed to the enhanced separation of photogenerated electron/hole carriers [11–16]. For gas-sensing applications, the effective integration of p- and n-type semiconductors can also provide higher sensing responses because of the formation of a deeper extended depletion layer [17–22]. To date, some nanocomposites of p- and n-type semiconductors such as CuO/SnO_2 [20], CuO/ZnO [21], and NiO/ZnO [22] have been prepared and investigated.

Spinel oxide Co_3O_4 is an important magnetic *p*-type semiconductor with an indirect band gap of 1.5 eV, and has been widely applied in lithium-ion batteries, gas sensing, heterogeneous catalysis, electrochemical devices, and other various applications [23–28]. To optimize the performance of Co_3O_4, a large amount of research during the past few years has focused on morphology and size control of Co_3O_4 [29–36]. Although great progress has been made, the improved performance of the developed Co_3O_4 with novel morphologies is still unable to meet the demand of

* Corresponding author. Tel.: +86 511 85638920; fax: +86 511 85635850.
E-mail address: aihuayuan@163.com (A. Yuan).

0169-4332/$ – see front matter © 2012 Elsevier B.V. All rights reserved.
http://dx.doi.org/10.1016/j.apsusc.2012.11.016

various practical applications. Recently, Na et al. [17] reported the preparation of Co_3O_4-decorated ZnO nanowire networks through a vapor phase route and found that they exhibited higher sensing selectivity. Gasparotto et al. [37] also investigated the gas-sensing properties of a multilayer Co_3O_4 and ZnO film. However, to the best of our knowledge, no report exists regarding the decoration of ZnO on Co_3O_4 for gas sensing.

In this study, an easy wet-chemistry route was developed for the fabrication of Co_3O_4/ZnO nanocomposites without the assistance of any organic additive or surfactant. First, Co_3O_4 nanostructures were prepared using $Co_2(OH)_2(CO_3)\cdot 22H_2O$ as a precursor. Then, to obtain Co_3O_4/ZnO nanocomposites, Co_3O_4 nanostructures were dipped in aqueous solution of $Zn(CH_3COO)_2$, followed by separation and calcination. During calcination, the adsorbed $Zn(CH_3COO)_2$ on the surface of the Co_3O_4 nanostructures is pyrolyzed into ZnO nanoparticles. Finally, the obtained Co_3O_4/ZnO nanocomposite was then fabricated into gas sensors, and the sensing performance was systemically investigated and compared with those of pure Co_3O_4 nanostructure and commercial Co_3O_4 powder. It was found that the Co_3O_4/ZnO nanocomposite showed a much higher sensing response than pure Co_3O_4 nanostructure, commercial Co_3O_4 powder, and pure ZnO sample.

2. Experimental details

2.1. Preparation of Co_3O_4 nanostructures

All reagents are of analytical grade, and were used as received. In a typical procedure, 2.5 g of $Co(CH_3COO)_2\cdot 4H_2O$ was dissolved in 30 mL of ethylene glycol to form a solution. The solution was heated in an oil bath at 160 °C (the solution's temperature is roughly 140 °C). 100 mL of Na_2CO_3 aqueous solution (0.2 mol/L) was then added to the solution. The obtained mixture was aged under stirring for about 30 min. The generated solid precursor (cobalt carbonate hydroxide) was then separated by centrifugation, thoroughly washed with ethanol and deionized water (five cycles), and dried in a vacuum. To obtain Co_3O_4 nanostructures, the as-synthesized precursor was heated at 450 °C in air for 4 h, and then cooled down naturally to room temperature.

2.2. Preparation of Co_3O_4/ZnO nanocomposites

50 mg of the as-prepared Co_3O_4 sample was first dispersed in 10 mL of $Zn(CH_3COO)_2$ aqueous solution (1 mol/L) through sonication. The resulting slurry was placed overnight. The solid was then separated by centrifugation, washed once with water, and dried in a vacuum. The dried product was then calcined at 500 °C in air for 0.5 h to form Co_3O_4/ZnO nanocomposites.

2.3. Characterizations

The phase structure of the as-obtained materials were examined using an X-ray powder diffractometer (XRD, CuK_α radiation, Shimadzu; $\lambda = 1.5406$ Å). The morphologies and dimensions of the samples were investigated using a Hitachi S-4800 field emission scanning electron microscope (SEM), and a JEOL-2100 high-resolution (HR-) transmission electron microscope (TEM), which was also used for the selected area electron diffraction (SAED) analysis (accelerating voltage of 200 kV). Energy-dispersive X-ray spectroscopy (EDS) data were also obtained on the JEOL-2100 TEM system. The gas-sensing test was performed on a commercial HW-30 gas-sensing measurement system (HanWei Electronics Co., Ltd., Henan, China) at a relative humidity of 20%–35%. The structure, fabrication, and testing principle of our gas-sensors are similar to our previously reported ZnO-based sensor [7,38]. The sensing response

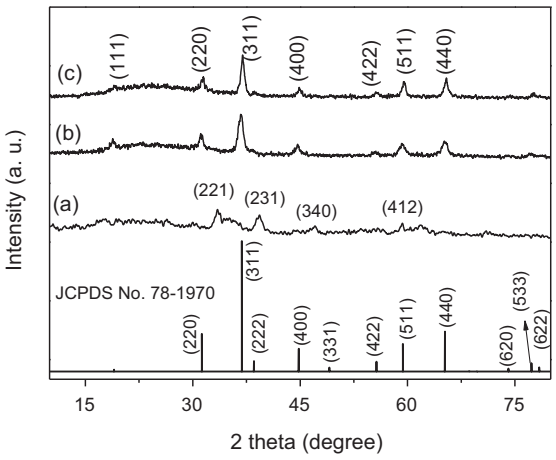

Fig. 1. XRD patterns of the as-prepared (a) $Co_2(OH)_2(CO_3)\cdot 22H_2O$, (b) Co_3O_4 obtained after thermal treatment, (c) Co_3O_4/ZnO nanocomposites. The standard data of cubic Co_3O_4 (JCPDS No: 42-1467) is also shown for comparison.

(S) was determined as the ratio R_g/R_a, where R_a is the resistance in ambient air, and R_g is the resistance in the tested gas atmosphere.

3. Results and discussion

3.1. Co_3O_4 nanostructures

The phase structure of the as-synthesized precursor sample was first examined by XRD. The XRD pattern is shown in Fig. 1a. All the observed diffraction peaks can be indexed to orthorhombic $Co_2(OH)_2(CO_3)\cdot 22H_2O$ (JCPDS No.: 48-0083). The peaks at $2\theta = 33.4$, 39.2, 47.0 and 59.2° originate respectively from the (2 2 1), (2 3 1), (3 4 0) and (4 1 2) crystal planes of orthorhombic $Co_2(OH)_2(CO_3)\cdot 22H_2O$. Fig. 1b shows that the Co_3O_4 (face-centered cubic, JCPDS No: 42-1467) is produced after thermal treatment of the as-obtained $Co_2(OH)_2(CO_3)\cdot 22H_2O$ at 450 °C for 4 h. The peaks can be attributed to the (1 1 1), (2 2 0), (3 1 1), (4 0 0), (4 2 2), (5 1 1), and (4 4 0) crystal planes of cubic phase Co_3O_4. No other peaks apart from those of Co_3O_4 were detected, thus verifying the complete conversion of cobalt carbonate hydroxide to Co_3O_4. The wide diffraction peaks suggest the small size of the obtained Co_3O_4. The XRD pattern of Co_3O_4/ZnO nanocomposite does not show obvious ZnO diffraction peaks, probably owing to the small content of ZnO in the nanocomposites (Fig. 1c).

The size and morphology of the precursor product were then examined by TEM and HR-TEM. As shown in Fig. 2a and b, the TEM images of $Co_2(OH)_2(CO_3)\cdot 22H_2O$ show one-dimensional nanostructures with lengths of 50 nm to 120 nm and diameters of approximately 8 nm. It seems that the one-dimensional nanostructures are formed by the curling of nanosheets. The HR-TEM observation shows the weak crystalline nature of one-dimensional nanostructures, which agrees with the XRD result. Fig. 2b exhibits the HR-TEM image of one $Co_2(OH)_2(CO_3)\cdot 22H_2O$ nanostructure. The corresponding fast Fourier transform (FFT) analysis of the noted area (inset of Fig 2b) yields a weak dot pattern from which the enhanced image is fabricated (inset of Fig 2b). The enhanced fringes can be indexed into the (0 4 0) and (2 2 1) crystal planes of $Co_2(OH)_2(CO_3)\cdot 22H_2O$. The formation of one-dimensional $Co_2(OH)_2(CO_3)\cdot 22H_2O$ nanostructure is possibly related to its layered crystal structure, which enables the easy formation of sheet-like nanostructures. The sheet-like nanostructures would curl to minimize their surface energy, and thus one-dimensional nanostructures are produced.

For the synthesis of Co_3O_4 nanostructures, the as-synthesized $Co_2(OH)_2(CO_3)\cdot 22H_2O$ products were heated at 450 °C in air for

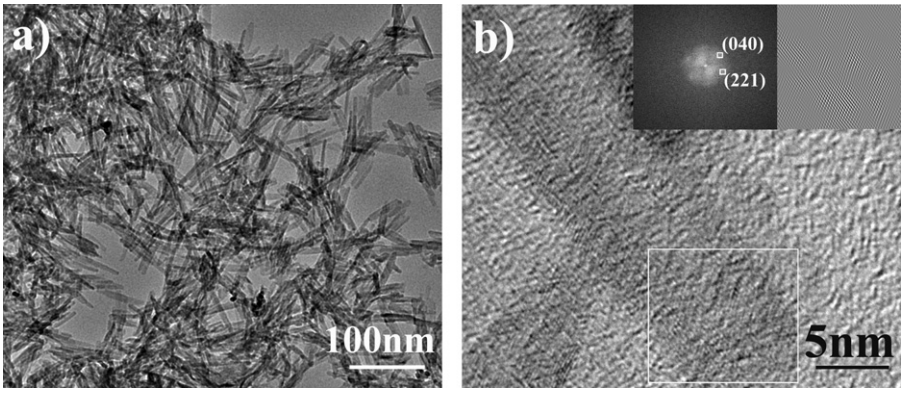

Fig. 2. (a) TEM image of as-synthesized $Co_2(OH)_2(CO_3)\cdot 22H_2O$ precursor showing rod-like structural features. (b) HR-TEM image of a rod-like structure. Insets denote the corresponding FFT analysis of the noted area and the sharpened fringes showing the (0 4 0) and (2 2 1) crystal planes of $Co_2(OH)_2(CO_3)\cdot 22H_2O$.

4 h. Fig. 3a shows the field emission (FE) SEM image of the synthesized Co_3O_4 nanostructures. The product comprises strings of Co_3O_4 nanoparticles with lengths of 20-50 nm and diameters of *ca.* 8 nm. The morphology and diameter of the Co_3O_4 nanostructures are somewhat inherited from the $Co_2(OH)_2(CO_3)\cdot 22H_2O$ precursor, whereas the length is much smaller than that of the precursor. The TEM image (Fig. 3b) further confirms that the Co_3O_4 one-dimensional nanostructures are actually the strings of Co_3O_4 nanoparticles. During calcination, the one-dimensional $Co_2(OH)_2(CO_3)\cdot 22H_2O$ precursor was decomposed into strings of Co_3O_4 nanoparticles, probably due to the release of water and carbon dioxide in the decomposition process, which could cause the nanorods to crack into the strings of nanoparticles. The SAED pattern (inset of Fig. 3b) recorded on many Co_3O_4 nanostructures shows bright diffraction rings, which can be easily attributed to the (1 1 1), (2 2 0), (3 1 1), and (4 0 0) lattice planes of cubic Co_3O_4. The sharp rings of the SAED pattern suggest high crystallinity of the Co_3O_4 product. Fig. 3c shows the HR-TEM image of the Co_3O_4 nanostructures. The easily observed lattice fringe spacings of 0.47 nm and 0.29 nm are attributed to the $d_{(1\text{-}1\,1)}$ and $d_{(2\,2\,0)}$ of cubic Co_3O_4.

3.2. Co_3O_4/ZnO nanocomposites

To prepare Co_3O_4/ZnO nanocomposites, we dispersed the obtained strings of Co_3O_4 nanoparticles in an aqueous solution of $Zn(CH_3COO)_2$, followed by separation, drying, and calcination. After calcination, the $Zn(CH_3COO)_2$ adsorbed on the surface of Co_3O_4 is decomposed into ZnO, thus forming Co_3O_4/ZnO nanocomposites. As shown in Fig. 4a, the obtained composites exhibit a particle-like shape, suggesting that the attachment of ZnO nanoparticles on the strings of Co_3O_4 nanoparticles decreases the length to diameter ratio of the resulting nanostructures. In addition, the strong sonication during the dispersion of Co_3O_4 nanostrings in the $Zn(CH_3COO)_2$ aqueous solution would also break the strings into nanoparticles. The TEM image (Fig. 4b) shows the same result as the SEM; however, differentiating Co_3O_4 and ZnO in the composites from the TEM image is difficult since Co_3O_4 and ZnO have almost the same electron density and contrast. The HR-TEM analysis of lattice fringe spacing enables the identification of the ZnO and Co_3O_4 phases. As shown in Fig. 4c, the hetero-interface of ZnO and Co_3O_4 is clearly observed, and the lattice fringe spacings of 0.47 nm and 0.26 nm originate from $d_{(1\,1\,1)}$ of cubic Co_3O_4 and $d_{(0\,0\,2)}$ of hexagonal ZnO, respectively. A pictorial model showing the composite nanostructures is demonstrated in Fig 4d. Considering the nano-level integration of a p-type (Co_3O_4) and an n-type semiconductor (ZnO), the obtained Co_3O_4/ZnO nanocomposites would have enhanced sensing properties.

The elemental composition of the Co_3O_4/ZnO nanocomposites is further determined by the EDS. The pristine Co_3O_4 sample shows the peaks from carbon, copper, cobalt, oxygen, and silicon elements (Fig. 5), in which carbon, copper, and silicon are from the background including the carbon-coated copper grid, which supports the sample. For the Co_3O_4/ZnO nanocomposite, the EDS pattern shows the existence of zinc apart from the above elements, suggesting the presence of ZnO composition in the composites. The semi-quantitative analysis of the nanocomposite by EDS shows the atomic ratio of Zn/Co = 1.0:7.9.

3.3. Gas-sensing properties

The gas-sensing properties of the as-prepared Co_3O_4 nanostrings and Co_3O_4/ZnO nanocomposites were investigated with formaldehyde and ethanol as model gases. For comparison, gas sensor based on commercial Co_3O_4 powder was also fabricated and tested.

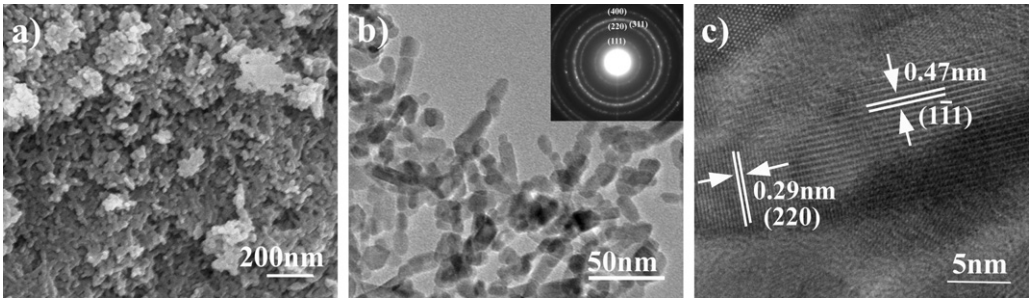

Fig. 3. (a) FE-SEM, (b) TEM, and (c) HR-TEM images of the as-synthesized Co_3O_4 one-dimensional nanostructures. The inset of (b) shows the SAED pattern recorded on Co_3O_4 nanostructures.

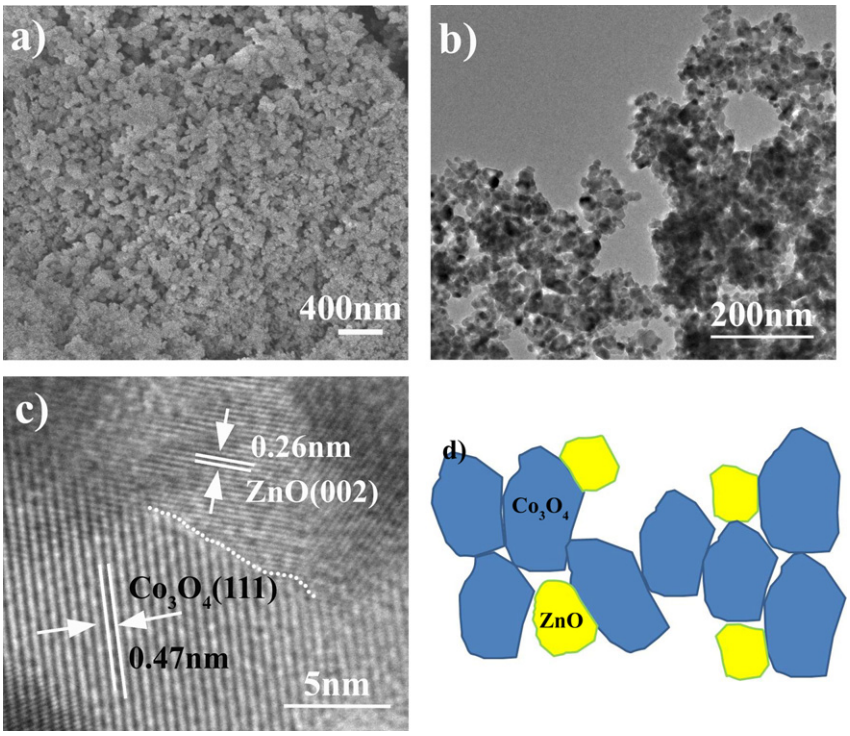

Fig. 4. (a) FE-SEM, (b) TEM, and (c) HR-TEM images of the as-synthesized Co_3O_4/ZnO nanocomposites. (d) Schematic model of the nanocomposite.

The sensing properties are highly dependent on operating temperature because of the temperature-dependent adsorption–desorption property of gas on sensing materials [39,40]. Therefore, we first investigated the influence of operating temperature on sensing response, which is defined as the ratio of R_g/R_a, where R_a is the resistance in ambient air, and R_g is the resistance in the tested gas atmosphere. To determine the optimum operating temperature, the response of Co_3O_4 nanostring gas sensor to 100 ppm of formaldehyde was tested as a function of operating temperature between 100 and 250 °C. This result indicates that the sensing response varies with the operating temperatures and a peak appears at approximately 180 °C. Similarly, the optimum operating temperature of 170 °C is obtained for the sensor to ethanol.

The real-time responses of the three sensors based on commercial Co_3O_4, Co_3O_4 nanostrings, and Co_3O_4/ZnO nanocomposites upon exposure to formaldehyde at 180 °C using air as the reference gas is shown in Fig. 6a. Unlike that of n-type semiconductors, the resistance of our prepared sensors increases upon exposure to reducing gases [1,2], suggesting a p-type semiconductor feature. This agrees well with the finding that Co_3O_4 is a typical *p*-type semiconductor [41]. The sensor resistance recovers almost to the initial value when the test chamber was refreshed with air. Although ZnO is a typical n-type semiconductor, the integration of ZnO with Co_3O_4 does not change the variation trend of the sensor's resistance when exposed to reducing gas. The response magnitude of the sensors improves dramatically with increasing concentrations of test gases. The response is highest with Co_3O_4/ZnO nanocomposite, followed by Co_3O_4 nanostrings and commercial Co_3O_4. This result reveals that Co_3O_4/ZnO nanocomposites have the best sensing performance. The response of Co_3O_4/ZnO nanocomposite sensor to 100 ppm of formaldehyde is 20. This value is four times the response obtained with the Co_3O_4 nanostring (4.4), and is much higher than that obtained with commercial Co_3O_4 powder (1.5). The obtained sensing response is also higher than that of our pure ZnO sample (4.1) [7], suggesting that the integration of Co_3O_4 and ZnO can effectively improve their gas sensing performance. The sensing responses of the three sensors as a function of formaldehyde concentration from 10 ppm to 200 ppm are shown in Fig. 6b. It can be seen that the responses of all the sensors follow an almost linear increase with increasing formaldehyde concentration in the range of 10–200 ppm.

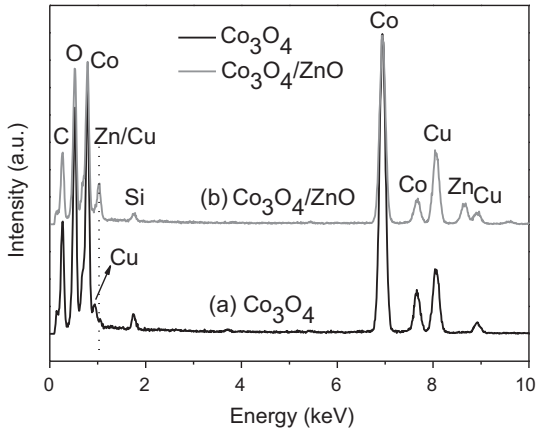

Fig. 5. EDS results of (a) the as-synthesized Co_3O_4 and (b) the Co_3O_4/ZnO nanocomposites.

The response characteristic curves of the three sensors to ethanol were also tested at the optimum operating temperature of 170 °C (Fig. 6c). Similarly, the Co_3O_4/ZnO nanocomposite sensor exhibits the highest response to ethanol. The response of Co_3O_4/ZnO nanocomposite sensor to 100 ppm of ethanol is 46, whereas those of Co_3O_4 nanostrings and commercial Co_3O_4 powder are 6.2 and 1.6, respectively. This response value (46) of Co_3O_4/ZnO nanocomposite sensor is also higher than the sensing response (7.5) obtained with pure ZnO sample [7]. The responses also exhibit a nearly linear increase with increasing ethanol concentration. But it seems that the Co_3O_4/ZnO nanocomposite sensor gradually becomes saturated saturation when the ethanol concentration is

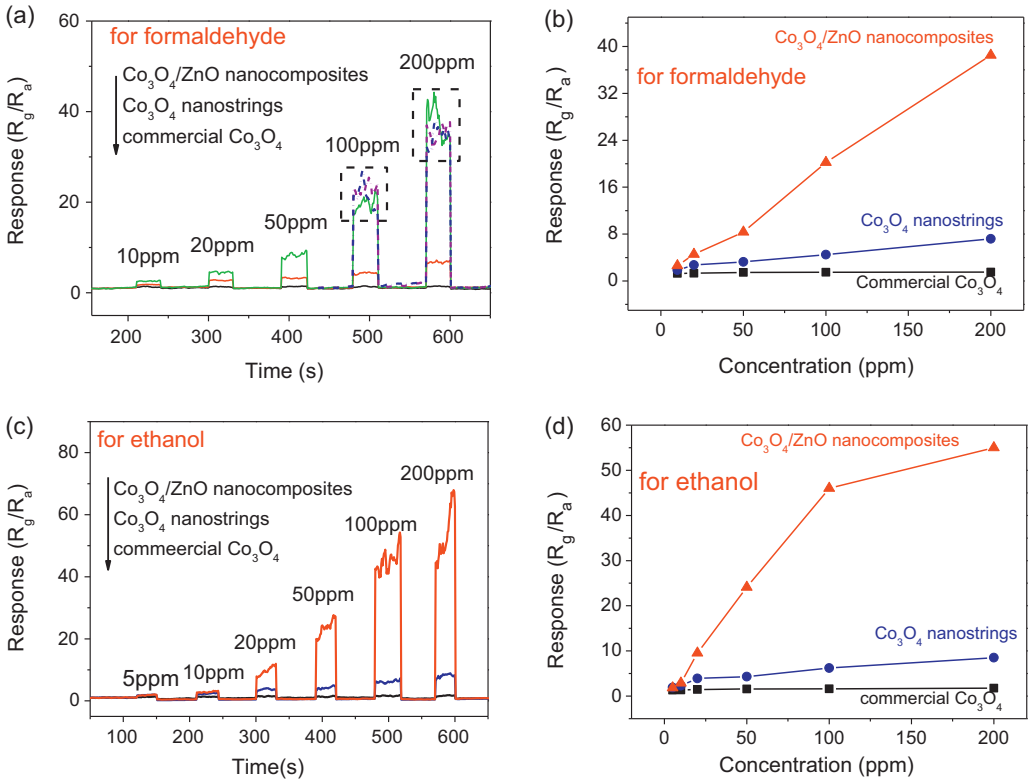

Fig. 6. Dynamic response-recovery curves of the three sensors based on commercial Co_3O_4, Co_3O_4 nanostrings, and Co_3O_4/ZnO nanocomposites to (a) formaldehyde and (c) ethanol. (b) and (d) show the gas concentration-dependent responses toward formaldehyde and ethanol, respectively. In the marked zone of (a), the response-recovery curves of another two gas sensors fabricated from Co_3O_4/ZnO nanocomposites to 100 ppm and 200 ppm of formaldehyde are denoted by dashed lines.

bigger than 100 ppm. It is believed that there is an optimum ratio of the two compositions for the best sensing properties [19]. In our case, the sensing properties are not fully optimized from the ratio of Zn to Co. It is believed that higher response would be obtained by tune it. The study on this issue is underway in our lab.

Furthermore, the almost complete recovery of baseline conductance values for the two tested analytes at the end of each pulse indicates a reversible interaction between sensing materials and target analytes. This is a key issue in view of eventual technology applications. The response characteristic curves display a noisy/unstable response when exposed to tested gases, especially at higher concentrations. As shown in the marked area of Fig. 6a, repeated tests from another two sensors fabricated with the same Co_3O_4/ZnO nanocomposites also yield similar results. In the sensors, bad electrical contacts would exist between parts of nanoparticles (Co_3O_4 and ZnO). These bad electrical contacts may cause electrical noises and induce noisy/unstable responses.

The sensing mechanism of an oxide is explained by ion-sorption. Ion-sorption is defined as the chemisorption of oxygen molecules on a sensing material's surface, resulting in negatively charged oxygen species. In our case, the main sensing material is Co_3O_4. Initially, the surface of Co_3O_4 in air is saturated with negatively charged oxygen species. When the testing system is exposed to analytes (such as ethanol), the oxygen species on Co_3O_4 promote the oxidation of test gas molecules to CO_2 and H_2O and the release of electrons, which induce changes in conductance. When ZnO is integrated with Co_3O_4 to form nanocomposites, p–n heterojunctions are formed at the interface between ZnO and Co_3O_4. At the p–n heterojunctions, oxygen-deficient ZnO shows *n*-type conductivity with electrons, whereas oxygen-excess Co_3O_4 shows p-type conductivity by holes. Some reports have shown that an effective p–n junction can enhance sensing properties [17,23–25,42]. The heterojunction region of Co_3O_4/ZnO is believed to easily attract reductive and oxidative gases (O_2), thus forming a deeper electron-depletion layer and causing a much higher sensing response than pristine oxides.

4. Conclusion

Co_3O_4/ZnO nanocomposites were synthesized by a simple and effective route without the use of any organic additive or surfactant. Extensive characterization by SEM, HR-TEM, EDS, and SAED shows intimate contact between the two oxides. The proposed method can be easily scaled-up for various applications. Preliminary tests with ethanol and formaldehyde as model analytes verify the improved sensing performance of Co_3O_4/ZnO nanocomposites, which can be attributed to the p–n junction effect of ZnO and Co_3O_4. The results demonstrate a promising approach to the development and realization of a low-cost and high-performance gas sensor based on a p-type semiconductor.

Acknowledgements

The authors are grateful for financial support from the Startup Fund for Distinguished Scholars (No. 35211103, 33211103), China Postdoctoral Science Foundation (2011M500085), Jiangsu Postdoctoral Science Foundation (1102001C).

References

[1] A. Tricoli, M. Righettoni, A. Teleki, Angewandte Chemie International Edition 49 (2010) 7632.
[2] M. Tiemann, Chemistry – A European Journal 13 (2007) 8376.
[3] J. Zhai, L. Wang, P. Wang, H. Li, Y. Zhang, D. He, T. Xie, ACS Applied Materials & Interfaces 32 (2011) 253.
[4] M. Ahmad, J. Zhu, Journal of Materials Chemistry 21 (2011) 599.

[5] Y. Zhang, W.u. Fu, Y. Sui, H. Yang, J. Cao, M. Li, Y. Li, X. Zhou, Y. Leng, W. Zhao, H. Chen, L. Zhang, Q. Jing, H. Zhao, Applied Surface Science 257 (2011) 5784.
[6] G.X. Zhu, C. Xi, H. Xu, D. Zheng, Y. Liu, X. Xu, X. Shen, RSC Advances 2 (2012) 4236.
[7] G.X. Zhu, Y. Liu, H. Xu, Y. Chen, X. Shen, Z. Xu, CrystEngComm 14 (2012) 719.
[8] X. Xue, Z. Chen, L. Xing, C. Ma, Y. Chen, T. Wang, Journal of Physical Chemistry C 114 (2010) 18607.
[9] X. Liu, J. Zhang, L. Wang, T. Yang, X. Guo, S. Wu, S. Wang, Journal of Materials Chemistry 21 (2010) 349.
[10] U. Choi, G. Sakai, K. Shimanoe, N. Yamazoe, Sensors and Actuators B 107 (2005) 397.
[11] Z.Y. Zhang, C.L. Shao, X.H. Li, C.H. Wang, M.Y. Zhang, Y.C. Liu, ACS Applied Materials & Interfaces 2 (2010) 2915.
[12] J.H. Hsieh, P.W. Kuo, K.C. Peng, S.J. Liu, J.D. Hsueh, S.C. Chang, Thin Solid Films 516 (2008) 5449.
[13] H.G. Kim, P.H. Borse, W.Y. Choi, J.S. Lee, Angewandte Chemie International Edition 44 (2005) 4585.
[14] L.J. Zhuge, X.M. Wu, Z.F. Wu, X.M. Yang, X.M. Chen, Q. Chen, Materials Chemistry and Physics 120 (2010) 480.
[15] K. Vanaja, U. Bhatta, R. Ajimsha, S. Jayalekshmi, M. Jayaraj, Bulletin of Materials Science 31 (2008) 753.
[16] S. Chen, W. Zhao, W. Liu, H. Zhang, X. Yu, Chemical Engineering Journal 155 (2009) 466.
[17] C.W. Na, H.S. Woo, I.D. Kim, J.H. Lee, Chemical Communications 47 (2011) 5148.
[18] A. Chowdhuri, P. Sharma, V. Gupta, K. Sreenivas, K.V. Rao, Journal of Applied Physics 92 (2002) 2172.
[19] Z. Wang, Z. Li, J. Sun, H. Zhang, W. Wang, W. Zheng, C. Wang, Journal of Physical Chemistry C 114 (2010) 6100.
[20] J. Tamaki, T. Maekawa, N. Miura, N. Yamazoe, Sensors and Actuators B 9 (2010) 205.
[21] Y. Nakamura, N. Yoshioka, M. Miyayama, H. Yanagida, T. Tsurutani, Y. Nakamura, Journal of the Electrochemical Society 137 (1990) 940.
[22] R.A. Marra, Y. Nakamura, S. Fujitsu, H. Yanagida, Journal of the American Ceramic Society 69 (1986) c143.
[23] J. Ma, A. Manthiram, RSC Advances 2 (2012) 3187.
[24] J. Xu, P. Gao, T. Zhao, Energy & Environmental Science 5 (2012) 5333.
[25] S. Xiong, J. Chen, X. Lou, H. Zeng, Advanced Functional Materials 22 (2012) 861.
[26] A. Cao, J. Hu, H. Liang, W. Song, L. Wan, X. He, X. Gao, S. Xia, Journal of Physical Chemistry B 110 (2006) 15858.
[27] W.Y. Li, L.N. Xu, J. Chen, Advanced Functional Materials 15 (2005) 851.
[28] Z.Q. Yuan, H. Chen, C. Li, L. Huang, X. Fu, D. Zhao, J. Tang, Applied Surface Science 255 (2009) 9493.
[29] J. Feng, H.C. Zeng, Chemistry of Materials 15 (2003) 2829.
[30] Y.G. Li, B. Tan, Y.Y. Wu, Nano Letters 8 (2008) 265.
[31] B. Wang, T. Zhu, H.B. Wu, R. Xu, J.S. Chen, X.W. Lou, Nanoscale 4 (2012) 2145.
[32] Q.Y. Yan, X.Y. Li, Q.D. Zhao, G.H. Chen, Journal of Hazardous Materials 209 (2012) 385.
[33] Y. Liu, Z. Zhang, S. Xiao, C. Qiang, L. Tian, J. Xu, Applied Surface Science 257 (2011) 7678.
[34] Y.J. Feng, L. Li, S.F. Niu, Y. Qu, Q. Zhang, Y.S. Li, W.R. Zhao, H. Li, J.L. Shi, Applied Catalysis B: Environmental 111 (2012) 461.
[35] Y.G. Li, B. Tan, Y.Y. Wu, Journal of the American Chemical Society 128 (2006) 14258.
[36] N. Yan, L. Hu, Y. Li, Y. Wang, H. Zhong, X.Y. Hu, X.K. Kong, Q.W. Chen, The Journal of Physical Chemistry C 116 (2012) 7227.
[37] D. Bekermann, A. Gasparotto, A. Barreca, C. Maccato, E. Comini, C. Sada, G. Sberveglieri, A. Devi, R.A. Fischer, ACS Applied Materials & Interfaces 4 (2012) 928.
[38] G.X. Zhu, H. Xu, Y. Liu, Z. Ji, X. Shen, Z. Xu, Sensors and Actuators B 166–167 (2012) 36.
[39] Z.P. Li, W.X. Pan, D.J. Zhang, J.H. Zhan, Chemistry—An Asian Journal 5 (2012) 1854.
[40] A. Pitois, A. Pilenga, A. Pfrang, G. Tsotridis, International Journal of Hydrogen Energy 36 (2011) 4375.
[41] H. Nguyen, S.A. El-Safty, Journal of Physical Chemistry C 115 (2011) 8466.
[42] L. He, Y. Jia, F. Meng, M. Li, J. Liu, Journal of Materials Science 44 (2009) 4326.